

PACS numbers: 42.55.Px; 42.60.Da; 42.60.Mi
DOI: 10.1070/QE2011v041n11ABEH014714

Spatio-temporal dynamics of a dual-wavelength vertical-external-cavity surface-emitting semiconductor laser

Yu.A. Morozov, A.I. Konyukhov, L.A. Kochkurov, M.Yu. Morozov

Abstract. **A mathematical model of a dual-wavelength vertical-external-cavity surface-emitting laser (VECSEL) is formulated with the distribution of optical pumping and generated fields over the beam cross sections taken into account. Dynamic regimes are mapped using the 'pump power – cavity round-trip time' plane. The map comprises regions of cw generation, periodic oscillation, quasi-periodic and chaotic oscillations of the radiation intensity and the carrier density in the active regions of the laser. It is shown that when the reflection coefficient of the external cavity is increased, the regions of complex dynamics in the maps become narrower. Using numerical methods the spatio-temporal dynamics of a dual-wavelength VECSEL is analysed in the regime of quasi-periodic oscillations.**

Keywords: *vertical-external-cavity surface-emitting laser, radiation dynamics, dual-wavelength semiconductor laser.*

1. Introduction

Semiconductor vertical-external-cavity surface-emitting lasers (VECSELs) have a special place among other sources of coherent radiation [1]. They combine the advantages of solid-state disk lasers based on rare-earth elements, i.e., generation of high-power radiation (up to tens of Watts) in a diffraction-limited Gaussian beam, and the advantages of semiconductor lasers, i.e., the possibility of selecting the oscillation frequency in a wide region depending on the composition and structure of active layers, the principal possibility of pumping by current, etc.

Realisation of the possibility to control the laser frequency by varying the parameters (molar composition) of the quantum wells in the same laser structure allowed a dual-wavelength semiconductor VECSEL to be fabricated [2]. This laser generating simultaneously two coaxial Gaussian beams at two wavelengths allows an efficient intracavity nonlinear-optical interaction that may give rise to radiation with combination frequencies, including the sum and difference ones. Radiation at the sum frequency with the wavelength ~507 nm was experimentally demonstrated in such a laser with a nonlinear lithium triborate (LBO) crystal placed inside the cavity [3]. However, the most attractive feature of the dual-wavelength VECSEL application is the generation of difference frequency, corresponding to the mid-IR region (5–50 μm). Despite the outstanding success of quantum-cascade lasers, construction of easy-to-use (without cryogenic cooling), relatively simple, low-cost radiation sources producing high-quality beams in this spectral region is still an urgent problem. First of all, this relates to the long-wavelength part of the mid-IR region.

In the course of the VECSEL fabrication and experimental study [2], it was found that the laser demonstrates different types of dynamic behaviour depending on the parameters of the pump and laser cavity. Particularly, it was found that, as the pump power grows starting from the threshold value, the laser, first, oscillates in the cw regime, and then, at a certain value of the pump power, switches over to the regime of pulsed oscillation. Later these features of the dynamic behaviour were confirmed and found physical interpretation within the framework of the mathematical model of a dual-wavelength VECSEL, formulated as a system of rate equations with delayed argument [4, 5].

Thus, the dual-wavelength VECSEL is a research object of interest both from fundamental point of view – as a nonlinear dynamical system with delayed argument – and from the applied one – as a device for efficient intracavity generation of difference-frequency harmonic in the long-wavelength part of the mid-IR spectral region.

In papers [4, 5] mentioned above, the mathematical model was reduced to the plane-wave approximation for the pump and generated radiation. Hence, some features of the oscillation process could not be taken into account. The present paper is devoted to the development of a more adequate mathematical model of the dual-wavelength VECSEL that takes into account the Gaussian transverse profile of both the generated waves and the pump, and to the analysis of VECSEL radiation dynamics in the spatio-temporal domain.

2. The laser scheme and mathematical model

The scheme of the laser is shown in Fig. 1. The laser cavity has V-configuration and consists of the active laser mirror, the folding spherical mirror and the output mirror in the geometry providing excitation of both generated wavelengths in the fundamental Gaussian mode. The laser is pumped by a 808-nm diode laser.

The main difference between the dual-wavelength VECSEL and the conventional one is the construction of the active laser mirror. Figure 2 presents its energy band diagram

Yu.A. Morozov, M.Yu. Morozov Kotel'nikov Institute of Radio Engineering and Electronics (Saratov Branch), Russian Academy of Sciences, ul. Zelenaya 38, 410019 Saratov, Russia;
e-mail yuri.mor@rembler.ru;
A.I. Konyukhov, L.A. Kochkurov N.G. Chernyshevsky Saratov State University, ul. Astrakhanskaya 83, 410012 Saratov, Russia;
e-mail: KonukhovAI@info.sgu.ru

Received 1 September 2011
Kvantovaya Elektronika **41** (11) 1040–1044 (2011)
Translated by V.L. Derbov

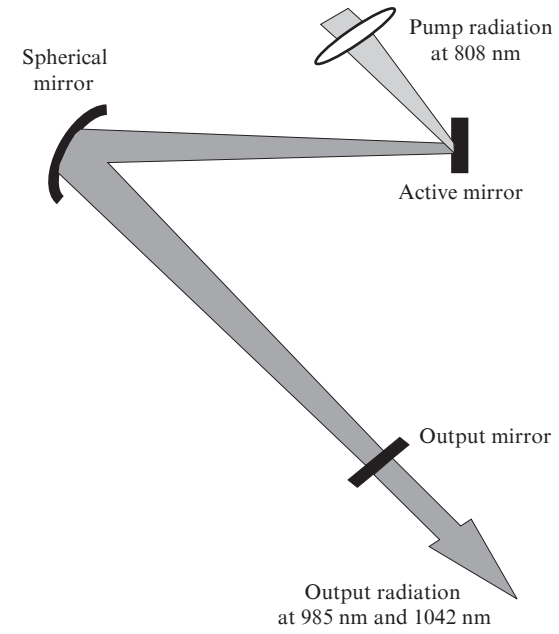

Figure 1. Scheme of the VECSEL.

schematically (not to scale). The mirror comprises at least two active regions, consisting of quantum wells (QWs) of different composition ($In_xGa_{1-x}As$ with different x), separated by GaAs barriers that serve as absorbers of the pump radiation. The active regions are separated from each other by a wide-band blocking AlAs layer that prevents diffusion transport of carriers, produced by the pump in these regions. This removes the problem of preferable population of deeper QWs due to smaller capture time and greater carrier emission time typical for these wells [6, 7].

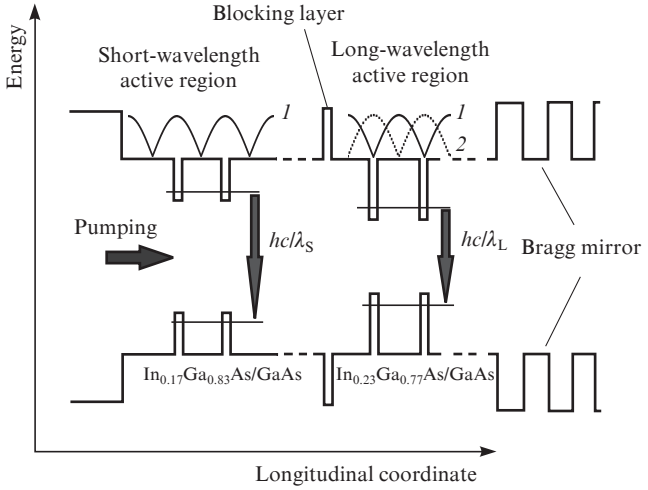

Figure 2. Energy band diagram of the active mirror; (*1*) and (*2*) are the distributions of amplitudes of short- and long-wavelength radiations, respectively.

The other important feature of the dual-wavelength VECSEL is that deep QWs are located approximately in the nodes of the standing wave of the short-wave radiation (see the amplitude distribution of the fields in the long-wavelength active region in Fig. 2). This provides the minimal level of absorption of the short-wavelength radiation in QWs and reduces the interaction between the short- and long-wavelength optical fields. At the same time both deep and shallow quantum wells are located at the antinodes of the standing wave of their 'own' field in order to provide the maximal use of the available gain. As in the conventional VECSEL, the reflection from the active mirror is provided by the Bragg mirror, in which the contrast between the refractive indices of the GaAs/AlAs layers is sufficient to provide reflection at both generated wavelengths (λ_S = 985 nm and λ_L = 1042 nm). A more detailed description of the laser construction may be found in [2].

Modification of the rate equations [5] describing the dynamics of a dual-wavelength VECSEL with the radial inhomogeneity of the pump and generated field taken into account [8] yields the following set of equations:

$$\dot{S}_i(t) = v_g\left\{\sum_{j=1}^{2}\Gamma_{ij}G_{ij}(t) - \alpha_i + \frac{1}{2L_i}\ln\left[\frac{S_i(t-\tau_{ext})}{S_i(t)}\right]\right\}S_i(t),$$
$$\dot{N}_i(t,r) = \frac{J_i(r)}{t_w} - \frac{N_i(t,r)}{\tau_r} - \frac{v_g}{m_i t_w}\sum_{j=1}^{2}\Gamma_{ji}g_{ji}L_j\frac{\psi_j^2}{\langle\psi_j^2\rangle}S_j(t). \quad (1)$$

Here the dynamic variables with the subscript $i = 1, 2$ refer to the short- and long-wavelength radiation, respectively; S_i is the density of photons; Γ_{ij}, g_{ij} are the longitudinal optical confinement coefficient and the local gain of the ith optical field in the jth equivalent quantum well; v_g is the group velocity; L_i is the effective length of the active mirror for the corresponding field; N_i is the carrier density in the equivalent QWs; τ_r and τ_{ext} are the lifetime in the QW and the external cavity round-trip time, respectively; $J_i(r) = J_{i0}\exp[-(r/w_p)^2]$ is the density of the pump-induced carrier diffusion flow into the ith QW; w_p is the pump beam radius; t_w is the QW width; m_i is the number of QWs in the appropriate active region; α_i is the absorption coefficient for the ith field. The modal gain for the field with the number i in the equivalent QW with the number j may be expressed as

$$G_{ij}(t) = \frac{1}{\langle\psi_i^2\rangle}\int_0^\infty g_{ij}(t,r)\psi_i^2 r\,dr,$$

where $\psi_i^2 = \exp[-(r/w_i)^2]$; $\langle\psi_i^2\rangle = \int_0^\infty \psi_i^2 r\,dr$; w_i is the beam radius for the ith field on the surface of the active mirror.

To derive Eqns (1), we used several simplifying assumptions, already used earlier in Ref. [5]. First, we considered one equivalent QW for each set consisting of m_i quantum wells of similar composition, keeping the same net gain for the ith field. This may be done by introducing a longitudinal optical confinement coefficient for each equivalent quantum well, accounting for the presence of all wells in the given set. Second, because for the laser under consideration the parameter of coupling of the active mirror with the external cavity is $\chi = r_{ext}(1 - r_f^2)/r_f \gg 1$, we did not take into account multiple reflections of radiation in the external cavity and, therefore, only the term $S_i(t - \tau_{ext})$, describing the density of photons after a single reflection from the external mirror, enters into Eqns (1) (here r_{ext} and r_f are the reflection coefficients of the external mirror and the internal surface of the active mirror). Moreover, we neglected the gain saturation caused by hole burning in the amplification spectrum, as well as the contribution of spontaneous emission into the laser modes. It

should be noted that the active regions of the laser containing the QWs of different molar composition become independent at $\Gamma_{12} = \Gamma_{21} = 0$. In other words, under these conditions the dual-wavelength VECSEL may be considered as an ensemble of two independent partial lasers, placed in one external cavity. The influence of the second of these conditions on the coupling of active regions in the VECSEL may be considered negligibly small, since only the combinations $\Gamma_{21}g_{21}$ enter Eqns (1), and the gain is $g_{21} \approx 0$. Therefore, below we assume $\Gamma_{21} = 0$. To find the relation between J_{i0} and the pump power, we used the approach thoroughly described in [9].

3. The results of calculations

The authors of [5] made a practically important conclusion that in the absence of coupling between the optical fields, i.e., when $\Gamma_{12} = \Gamma_{21} = 0$, the state of the dual-wavelength cw oscillation is stable. If for some reasons, e.g., inexact coincidence of the position of deep QWs with the short-wavelength field nodes, the laser radiation fields are coupled, the cw regime may lose stability after transition to self-modulation or pulsed oscillation.

The clearest presentation of possible types of behaviour of the dynamic system under study is provided by the regime map, i.e., the diagram drawn in the two-parameter plane, in which the regions, corresponding to different dynamic regimes, are indicated. To draw these maps we used the DDE-BIFTOOL software package [10] for numerical analysis of dynamic systems with delayed argument. Figure 3 shows the maps of dynamic regimes drawn in the plane of parameters P_{in}, τ_{ext} for $r_{ext}^2 = 0.98$ and 0.985. The rest parameters, used in the calculations, have the values: $L_1 = L_2 = 10$ μm, $\Gamma_{11} = \Gamma_{22} = 0.0112$, $\Gamma_{12} = \Gamma_{11}/5$, $\alpha_1 = \alpha_2 = 10$ cm^{-1}, $\tau_r = 2$ ns, $t_w = 7$ nm, $m_1 = m_2 = 8$, $w_1 = w_2 = w = 50$ μm, $w_p = 60$ μm. The local gains for QWs were calculated numerically [11] and expressed for convenience in the form of the following dependences: $g_{11} = 2200\ln[N_1(r)/1.9]$, $g_{21} = -1.216N_1^2(r) + 24.55N_1(r) - 59.765$, $g_{22} = 2250\ln[N_2(r)/2.04]$, $g_{12} = -47.64N_2^2(r) + 1236.2N_2(r) - 5288.8$. Here the volume carrier concentrations $N_{1,2}$ are normalised to 10^{18} cm^{-3}.

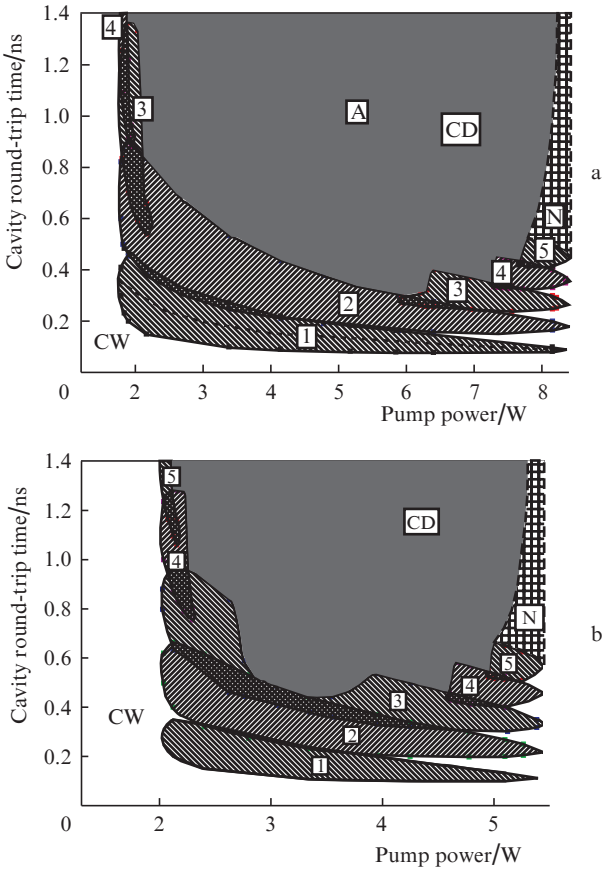

Figure 3. The map of dynamic regimes for the dual-wavelength VECSEL at $r_{ext}^2 = 0.98$ (a) and 0.985 (b).

White regions in the maps (Fig. 3), marked with CW (continuous wave), correspond to the intervals of variation of the pump power P_{in} and the round-trip time τ_{ext} of the external cavity, within which the laser operates in the cw oscillation regime. The origin of the abscissa axis approximately coincides with the threshold pump power for both generated wavelengths. It is seen that if the delay time τ_{ext} in the external cavity does not exceed approximately 0.1 ns, the cw dual-wavelength oscillation appears to be stable in the whole interval of the pump power variation.

When τ_{ext} exceeds 0.1 ns and the pump power becomes greater than 1.8 W (Fig. 3a) or 2 W (Fig. 3b), the stability of the stationary state (cw oscillation) gets broken and the dynamics of the system becomes more complex. The instability is due to the onset of relaxation oscillations, the frequency Q of which for independent active regions of the laser (i.e., for $\Gamma_{12} = 0$) was determined in [5] as $Q = \omega(2/\varepsilon)^{0.25}$, where ω is the angular frequency of the relaxation oscillations in the absence of the external cavity (nearly the same for both partial lasers), $\varepsilon = 1 - r_{ext}^2$ is the power transmission coefficient of the output mirror. In the presence of coupling between the oscillators, representing individual lasers, the eigenfrequency Q gives rise to two frequencies of normal oscillations $Q_{n1,2}$ [12]. The main features of the oscillations in this case are determined by the normal oscillations with minimal damping (suppose that the corresponding frequency is Q_{n1}). For weak coupling the difference between the normal oscillation frequencies and the frequency of relaxation oscillations is not large; therefore, qualitatively the character of the dependence of Q_{n1}, e.g., on ω, will not change. Hence, we may expect that $Q_{n1} \propto \omega \propto \sqrt{P_{in}/P_{th} - 1}$ (P_{th} is the threshold power) [11]. Besides, the presence of coupling between the active regions of the laser may lead to the growth of normal oscillations instead of their damping. In this case, as a result of Hopf bifurcation, a limit cycle is created in the phase space of the system with the frequency of revolution equal to that of the normal oscillations.

Within the shaded regions 1 – 5 in Fig. 3, the laser demonstrates stable periodic oscillations of the radiation intensity and the carrier density with the period T such that the delay time is an integer multiple of such periods, $T \approx \tau_{ext}/n$. The integer n numbers the corresponding regions in the map. In our opinion, the existence of stable periodic motions in the system with peculiar features presented in Fig. 3 may be explained within the framework of the concept of pulling (synchronisation) of the normal oscillation frequency by the frequency of intermode beats (for $n = 1$) or its harmonics (for $n > 1$).

Consider the behaviour of the dynamic system at a certain fixed value of the pump power and the increasing delay time τ_{ext} in the external cavity (i.e., the representation point moving along the ordinate axis). In region 1, we have $\Omega \approx \Omega_b$, where $\Omega = 2\pi/T$ is the angular frequency of the observed periodic oscillations, and $\Omega_b = 2\pi/\tau_{ext}$ is the angular frequency of

the intermode beats. Thus, while the representation point moves within region 1, the frequency Ω decreases. When the representation point passes to the adjacent region 2, the frequency Ω increases stepwise by two times to satisfy the condition $T \approx \tau_{ext}/2$. In the course of further increase in the time τ_{ext}, the frequency Ω decreases again.

If the pump power is chosen such that the representation point moving across the map crosses also other regions of periodical oscillation, the character of the frequency change repeats. Therefore, the physical picture of the dependence of the periodical oscillation frequency on the delay time τ_{ext} looks like a synchronisation process, in which the frequency of normal oscillations of the system becomes equal to the intermode frequency or its harmonics. When the pump power increases, the widths of the synchronisation regions of periodic oscillations decrease. Thus, for the pump power ~8.4 W (Fig. 3a) or 5.3 W (Fig. 3b) the regions shrink almost into a point. The value τ_{ext}, to which region 1 collapses, allows one to judge about the frequency of normal oscillations for the given pump power: $Q_{n1} = 2\pi/\tau_{ext}$. The variation of the normal oscillation frequency for other values of the pump power corresponds to the relation $Q_{n1} \propto \sqrt{P_{in}/P_{th} - 1}$, mentioned above, and is shown in Fig. 3a by a dotted line, crossing region 1.

It also follows from Fig. 3 that starting from $n = 3$ (Fig. 3a) or $n = 4$ (Fig. 3b) the regions of periodic motions of the system at small (1.8–2.3 W) and large (~8 W for Fig.3a and ~5 W for Fig. 3b) pump powers have a doubly connected character, i.e., they consist of two sub-regions, located near the boundaries of stability of the cw oscillation regime. Only the regions of periodic oscillations of the system up to $n = 5$ are mapped in detail. The periodic motions of the system with $n > 5$ fall into the regions, denoted as N and shown qualitatively.

One can see that the regions of periodic motions overlap in pairs. This means that within the regions of overlap the periodical oscillations of dynamic variables are possible with the period, corresponding to one or another of the overlapping regions, depending on the specified initial conditions. In other words, the overlap regions are regions in which the hysteresis of the oscillation period is possible depending on the direction, in which the representation point moves, crossing these regions.

In the CD (complex dynamics) region filled with grey in the map the complex quasi-periodic and, possibly, chaotic oscillations occur. Distinguishing between the quasi-periodic and chaotic motions requires the analysis of spectra of Lyapunov exponents for the attractor in the delayed system [13], which is beyond the scope of the present paper.

Comparison of Figs 3a and b shows how the map of dynamic regimes is modified with the growth of the reflection coefficient of the external mirror, namely, the regions of similar periodic, quasi-periodic and chaotic oscillations become narrower. Special analysis shows that if the reflection coefficient r_{ext} of the external mirror is increased up to 0.99, the cw operation regime of the dual-wavelength VECSEL keeps stable over the whole domain of variation in the pump power P_{in} and the delay time τ_{ext}.

Direct calculation of dynamic behaviour of the dual-wavelength VECSEL with the help of the set of equations (1) confirms the conclusions drawn from the bifurcation analysis. Figure 4 demonstrates the dynamics of radiation in the time interval, equal to a single period of oscillation, for the parameter values, corresponding to the point A of the map in Fig. 3a. According to the classification, presented above, a complex quasi-periodic regime of radiation with several incommensurable periods is observed at this point. Analysis shows that among these periods a period is sure to exist that is equal to the time τ_{ext} of the external cavity round-trip. The oscillations of the radiation power within this 1-ns-long period are shown in Fig. 4. Besides, the radiation intensity oscillations are modulated in much longer-time scale, with typical periods of a few hundreds of nanoseconds or even a few microseconds. It follows from Fig. 4 that the power oscillations of the long-wavelength radiation practically repeat those of the short-wavelength. The only difference is that the power is greater for the long-wavelength radiation, and that this radiation is slightly delayed in time with respect to the short-wavelength one. As shown in [14], the delay for which the radiation pulses at different frequencies remain considerably overlapping in time, does not hamper efficient generation of difference frequency as a result of intracavity nonlinear-optical conversion.

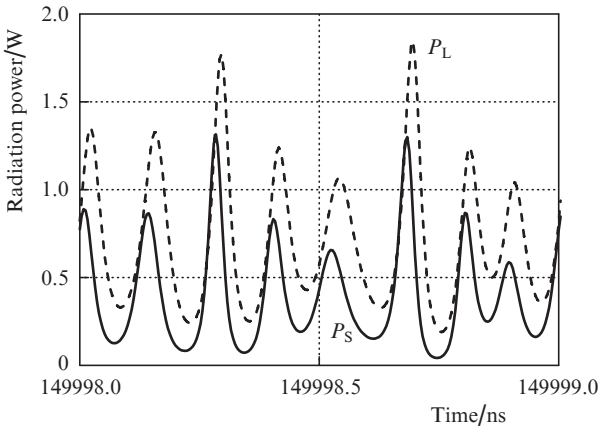

Figure 4. Radiation power of the short- (solid line) and long-wavelength (dashed line) radiation components in the time interval equal to one period.

In Fig. 5 in the form of level lines of equal concentration the spatio-temporal distribution of carriers in the QWs of the short-wave active region is shown for the same parameters and in the same time interval that were used in the calculation

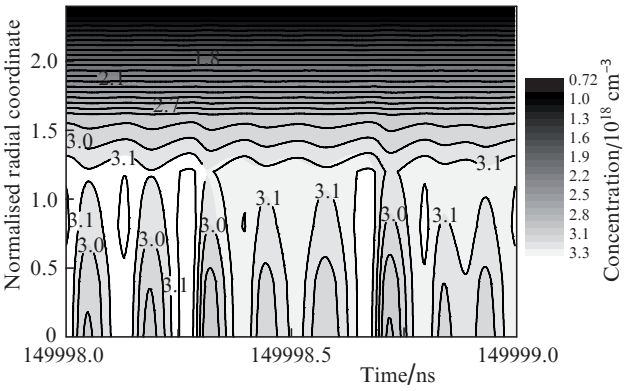

Figure 5. Spatio-temporal dynamics of the carrier concentration in the QWs of the short-wavelength active region. The labels in the plot correspond to the level lines of concentration normalised to 10^{18} cm^{-3}.

of the dependences, presented in Fig. 4. The vertical axis shows the values of the radial coordinate r scaled to the radius w of radiation beams. It is seen that the most significant temporary variations of the charge carrier concentration in the QWs are observed near the axis of the beam. These variations amounting to 10% of the mean value are caused by burning dips in the concentration profile by the optical radiation. Indeed, as the comparison of Fig. 4 and Fig. 5 shows, the greatest dips of near-axis concentration of carriers are observed at 149998.3 and 149998.7 ns, where the optical radiation power attains maximal values. Off the beam axis both the pulsation amplitude and the mean level of carrier concentration in the QWs decrease. This behaviour is quite predictable because of the accepted radial dependence of the pump power density (and, hence, the rate of carried production by the pump) and the radiation fields.

4. Conclusions

With the experimentally observed spatial distributions of the pump and optical radiation fields taken into account, the mathematical model of a dual-wavelength VECSEL is presented in the form of a set of rate differential equations with delayed argument. The bifurcation analysis of the dynamic behaviour of the dual-wavelength VECSEL is carried out and the maps of dynamic regimes are drawn in the plane of 'pump power – cavity round-trip time' parameters. In these maps the regions, corresponding to the cw steady-state oscillation, the generation of a pulse-periodic sequence with the period equal to the round-trip time divided by an integer, and the radiation regime with quasi-periodic (or chaotic) oscillations of intensity are determined. The synchronisation of relaxation oscillations by the frequency of intermode beats or its harmonics is proposed as a possible explanation of stable periodic motions in the considered dynamic system.

It is shown that when the reflection coefficient of the external mirror r_{ext} increases (the losses in the system decrease), the intervals of the pump power and delay time in the cavity, in which periodic, quasi-periodic or chaotic oscillations of the radiation intensity are observed, become narrower. For $r_{ext} = 0.99$ the system demonstrates only the cw oscillation.

Calculation of radiation dynamics, corresponding to Eqns (1), is carried out. It is found that among the variety of periodic motions, representing complex quasi-periodic (or chaotic) oscillations of the photon density and the density of charge carriers in QWs the motions with the period equal to the cavity delay time are sure to exist. A typical feature of quasi-periodic (chaotic) oscillations is also the presence of other motions with much longer time scales (having the periods from a few hundreds of nanoseconds to a few microseconds), which manifest themselves in modulation of fast oscillations. The transformation of quasi-periodic oscillations into chaotic ones occurs, probably, via complication of the quasi-periodic oscillations.

Analysis of spatio-temporal dynamics of the carrier distribution in QWs shows that the most significant variations in their concentration depending on time occur in the near-axis region of the beam. It is shown that these variations may be a result of spatio-temporal hole burning by the optical radiation.

Acknowledgements. The work was supported by the Russian Foundation for Basic Research (Grant No. 10-02-01074).

References

1. Tropper A.C., Foreman H.D., Carnache A., Wilcox K.G., Hoogland S.H. *J. Phys. D*, **37**, R75 (2004).
2. Leinonen T., Morozov Yu.A., Härkönen A., Pessa M. *IEEE Phot. Techn. Lett.*, **17**, 2508 (2005).
3. Härkönen A., Rautiainen J., Leinonen T., Morozov Yu. A., Orsila L., Guina M., Pessa M., Okhotnikov O. G. *IEEE Phot. Techn. Lett.*, **19**, 1550 (2007).
4. Morozov Yu. A., Leinonen T., Härkönen A., Pessa M. *IEEE J. Quantum Electron.*, **42**, 1055 (2006).
5. Morozov M.Yu., Morozov Yu.A., Krasnikova I.V. *Radiotekh. Elektron.*, **55**, 1243 (2010). [*J. Comm. Tech. Electron.*, **55**, 1162 (2010)].
6. Morozov M.Yu., Morozov Yu.A., Krasnikova I.V. *Pis'ma Zh. Tekh. Fiz.*, **34**, 80 (2008) [*Tech. Phys. Lett.*, **34**, 1034 (2008)].
7. Tsai C.-Y., Tsai C.-Y., Lo Y.-H., Spencer R., Eastman L. *IEEE J. Sel. Topics Quantum Electron.*, **1**, 316 (1995).
8. Valle A., Pesquera L. *J. Opt. Soc. Am. B*, **19**, 1549 (2002).
9. Morozov Yu., Leinonen T., Morozov M., Ranta S., Saarinen M., Popov V., Pessa M. *New J. Phys.*, **10**, 063028 (2008).
10. Engelborghs K., Luzyanina T., Samaey G. *DDE-BIFTOOL v.2.00 user manual: a Matlab package for bifurcation analysis of delay differential equations. Tehn. Rep. TW-330* (Leuven, Belgium, 2001) p. 60.
11. Zory P.S., Jr. (Ed.) *Quantum-well Lasers* (San Diego: Acad. Press, 1993).
12. Karlov N.V., Kirichenko N.A. *Kolebaniya, volny, struktury* (Oscillations, Waves, Structures) (Moscow: Fizmatlit, 2003) p. 31.
13. Farmer J.D. *Phys. 4D*, 366 (1982).
14. Morozov Yu.A., Morozov M.Yu., Krasnikova I.V. *Sbornik statey 8 Belorussko-Rossiyskogo seminara 'Poluprovodnikovye lasery i sistemy na ikh osnove'* (Book of Papers. 8th Belarus-Russia Workshop 'Semiconductor Lasers and Systems' (Minsk, 2011) pp 46–49.